# Magnetic sensitive force microscopy

**High-resolution magnetic imaging down to the atomic scale is of utmost importance to understand magnetism on the nanoscale and below. Here we report on recent advances in force microscopy based techniques from our laboratory, namely magnetic force microscopy and magnetic exchange force microscopy. The former is a well established technique for studying ferromagnetic domain patterns by sensing the long-range magnetostatic tip-sample interaction relatively far above the surface. In contrast, the latter is a novel and promising tool capable of detecting spin configurations with atomic resolution by probing the short-range magnetic exchange interaction at very small tip-sample distances. Data acquisition schemes and tip preparation methods are evaluated on sample systems to illustrate and compare sensitivity and spatial resolution of both methods.**

**Alexander Schwarz\* and Roland Wiesendanger**

*Institute of Applied Physics and Microstructure Research Center, University of Hamburg, Jungiusstrasse 11, D-20355 Hamburg, Germany*
*\*E-mail: aschwarz@physnet.uni-hamburg.de*

Developments toward high-resolution magnetic imaging are fueled by demands of modern magnetic data storage and sensor technologies, as well as a still intense interest in the fundamentals of magnetic phenomena. Over the past decades, a wide range of methods have been developed to image magnetic domain patterns, e.g. Bitter decoration technique[1], magneto-optical microscopy in reflection (Kerr effect) and transmission (Faraday effect)[2], Lorentz force microscopy[3], scanning electron microscopy with polarization analysis[4], and X-ray magnetic linear and circular dichroism microscopy[5]. In addition, many scanning probe techniques are magnetically sensitive, e.g. scanning Hall probe microscopy[6], scanning superconducting quantum interference device (SQUID) microscopy[7], magnetic force microscopy (MFM)[8], and spin-polarized scanning tunneling microscopy[9]. The newest addition to this family is magnetic exchange force microscopy (MExFM)[10].

It is beyond the scope of this article to discuss all these methods in detail; they all have their assets and drawbacks. In the following, we will focus on recent results and advances achieved in our laboratories using the two force microscopy based methods, i.e. the already mature

MFM and the novel MExFM. Both methods utilize an atomic force microscopy (AFM) set-up as introduced by Binnig et al.[11]. Its main feature is a force sensor comprising of a sharp tip mounted at the free end of a flexible cantilever that is scanned across a surface to detect the tip-sample interaction force locally.

MFM senses the dipolar magnetostatic force between a ferromagnetic tip and a ferromagnetic sample. Since the magnetostatic force is long range, typical tip-sample separations are larger than 10 nm. The practical reason for this large distance will become clear later. An important consequence is that the resolution is limited to the nanometer scale. Nevertheless, it is still a very powerful tool to study ferromagnetic domain patterns[12], domain walls[13,14], and magnetic vortices[15], as well as flux lines in superconductors[16,17]. The vast majority of all MFM experiments are performed in zero or rather small magnetic fields. By setting up a microscope that can be operated in an external flux density of up to 5 T[18], we have been able to observe the $B$-dependence of domain patterns in ferromagnetic thin films[19,20], as well as the $B$-dependence of static and dynamic flux-line configurations in high-temperature superconductors[21,22].

To exceed the nanometer resolution capabilities of MFM, it was proposed as early as 1990 by Wiesendanger et al.[23] to use the short-range magnetic exchange force for magnetic imaging. This force acts between two closely spaced atomic magnetic moments (spins) and hence can only be detected at very small tip-sample distances on the order of 0.5 nm. Theoretical calculations[24–27] predict the feasibility of obtaining magnetic sensitivity with atomic resolution, i.e. performing MExFM. However, until recently all experiments have failed to prove the suggested concept on NiO(001) without ambiguity[28,29], including measurements performed by ourselves[30,31]. The breakthrough came when we were able to manipulate the spin at the foremost tip atom into a favorable direction by applying a large external flux density[10].

## Force microscopy: set-up and modes of operation

All experiments presented in the following have been carried out in an ultrahigh vacuum (UHV) cryostat system setup on a separate foundation in a low noise environment. The home-built microscope (*Hamburg design*) is located in a liquid helium bath cryostat equipped with a superconducting magnet, which can generate a flux density $B$ of up to 5 T perpendicular to the sample surface[18]. Constant low temperatures, a rigid microscope design, and a low noise interferometric detection system account for high force sensitivity and stable imaging conditions even at very small tip-sample separations. In a preparation chamber attached to the cryostat, Si cantilevers[32] can be coated with magnetic materials to attain magnetic sensitivity. This is an important feature because it enables us to optimize the magnetic properties of the tip for each sample system. Such *in situ* preparation also circumvents all possible complications arising from oxidation and contamination of *ex situ* coated tips.

Numerous force microscopy operating modes do exist. Unfortunately, the nomenclature found in the literature is often inconsistent because naming emerged in the context of instrumental developments rather than describing the method adequately. In general, one can distinguish between dynamic and static modes, indicating whether the cantilever oscillates or not. It is further useful to distinguish between contact, cyclic contact, and pure noncontact modes to specify the tip-sample interaction regime. We employ the dynamic mode using the frequency modulation (FM) technique[33] in the pure noncontact (NC) regime, i.e. the oscillating tip always stays in the attractive regime of the tip-sample interaction. Unlike the contact regime, an atomically sharp tip can be maintained during imaging at small tip-sample separations. Using this operating mode, known as NC-AFM and FM-AFM, in UHV *true* atomic resolution becomes routine via the detection of short-range chemical interactions[34–36]. FM in vacuum is particularly advantageous because it offers high force sensitivity as a result of very large quality factors ($Q > 10\,000$) of the cantilever oscillation. Note that the force sensitivity scales with $\sqrt{Q}$ and that external damping arising from operation in air limits $Q$ to 300 or less.

Image recording in the FM mode is schematically shown in Fig. 1. A cantilever with eigenfrequency $f_0$ and force constant $c_z$ is oscillated by self-excitation and kept at a constant amplitude $A$ by a feedback loop (yellow components). Typical values of $f_0$, $c_z$, and $A$ in our experiments are 50–200 kHz, 1–40 Nm$^{-1}$, and 2–20 nm, respectively. Because of tip-sample interactions, its actual resonance frequency $f$ is shifted by $\Delta f$, i.e. $\Delta f = f - f_0$. Negative and positive $\Delta f$ indicate attractive and repulsive magnetostatic interactions, respectively.

In the constant frequency shift mode, $\Delta f$ and therefore the tip-sample interaction force are kept constant by a $z$-feedback loop (blue components), which adjusts the tip-sample distance in the $z$-direction accordingly during scanning in the $x$-$y$ plane across the surface. The resulting $z(x, y)$ image reflects the surface topography, revealing steps, terraces, adsorbates, etc. Suitable frequency shift set points depend on tip sharpness as well as spring constant, resonance frequency, and amplitude set point. For cantilevers, we use $\Delta f$ set points ranging from –0.5 Hz to –20 Hz. To obtain atomic resolution, larger negative frequency shifts have to be used to achieve smaller tip-sample distances. Height differences on the atomic scale correspond to variations of the short-range interatomic forces between tip and sample.

Another data acquisition scheme is the constant height plane-subtraction mode, which is used to record MFM data[18,37]. First, the tilt between tip and sample has to be compensated with active $z$-feedback. Thereafter, it is switched off and the tip is retracted to a certain height $h$. Since the tilt has been compensated, the tip is scanned in a constant height $h$ over the surface (Fig. 1b). $\Delta f(x, y)$-maps recorded in this so-called plane-subtraction mode reflect the magnitude and sign of the tip-sample interactions. Without tilt compensation, unwanted contrast variations would perturb the image data.
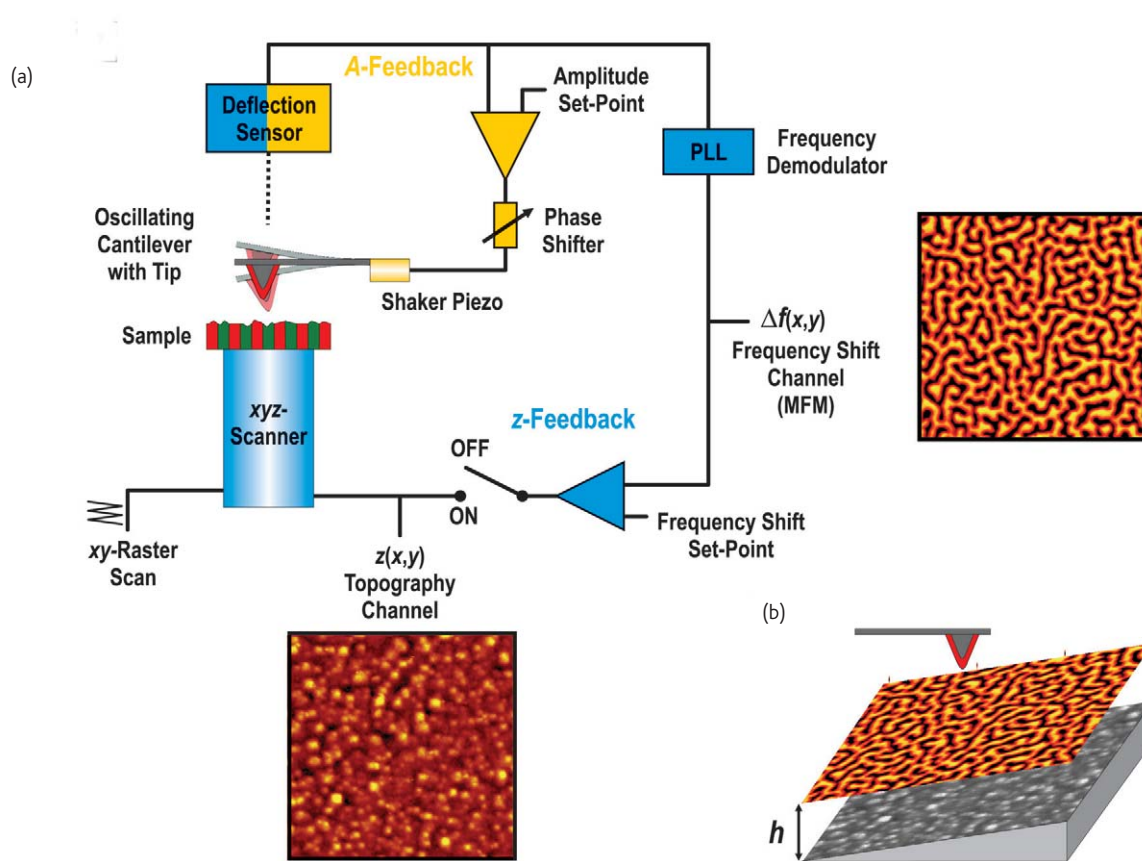
Fig. 1 (a) Force microscopy image recording using the frequency modulation technique. Blue and yellow components denote parts that belong to the amplitude- and z-feedback loop, respectively. The latter is active whenever the microscope is operated in the constant frequency shift mode to record data in the topography channel. The height information is color coded in such images. To record MFM data using the plane subtraction mode to scan in a constant height h, the z-regulator is switched off and the frequency shift channel is recorded in the form of color-coded images. (b) Illustration of the plane-subtraction mode. The topography (gray) is slightly tilted with respect to the tip. This tilt has to be compensated for in the constant frequency shift mode. Thereafter, image acquisition at a constant height h is possible.

# MFM: ferromagnetic domain imaging

## Separation of forces

The merit of force microscopy is its capability to detect all kinds of short- and long-range electromagnetic tip-sample interaction forces, e.g. electrostatic, magnetostatic, van der Waals, chemical, magnetic exchange, friction, adhesive, and elastic. However, the experimentalist is mostly interested in only one of these forces, e.g. the magnetostatic force in an MFM experiment. Therefore, one has to separate the topography and the magnetic signal. This can be done simply by scanning the tip relatively far above the surface ($h > 10$ nm) using the constant height plane-subtraction mode. At such a distance, the long-range tip-sample interactions, i.e. the magnetostatic and electrostatic interactions, dominate. The latter is often disregarded, but has to be considered to obtain a pure magnetostatic signal. An electrostatic contribution is present whenever tip and sample exhibit different work functions, $W_1$ and $W_2$, which results in a contact potential difference (CPD). To avoid any crosstalk between electrostatic and magnetostatic signals, the CPD has to be compensated by applying an appropriate

bias voltage, $U_{Bias} = -U_{CPD}$ with $eU = \Delta W = W_1 - W_2$, as shown in Fig. 2c. To determine $U_{CPD}$, a $\Delta f(U_{Bias})$-curve is recorded at a fixed $x,y$-position on the sample with the z-feedback loop switched off. The shape of the curve is parabolic (if tip and sample are well conducting) and the voltage at the apex corresponds to $U_{CPD}$.

Electrostatic crosstalk is particularly bothersome on rough surfaces because electric charges assemble there, resulting in a topography-like contrast even at relatively large tip-sample separations. The effect is demonstrated in Fig. 2 on a ferromagnetic sample with a grainy surface. A nonmagnetic tip is used to exclude any magnetostatic contribution to the tip-sample interaction. In Fig. 2a, the surface topography recorded in the constant frequency shift mode with compensated CPD is shown ($U_{Bias} = -U_{CPD} = +0.4$ V). Then an image in the constant height plane-subtraction mode ($h = 10$ nm) is recorded with four different values for $U_{Bias}$ (Fig. 2b). Only when the CPD is balanced (at +0.4 V) is no topography-like contrast visible. Note that the contrast at the other bias voltages must be of electrostatic origin, because its magnitude depends on $U_{Bias}$.
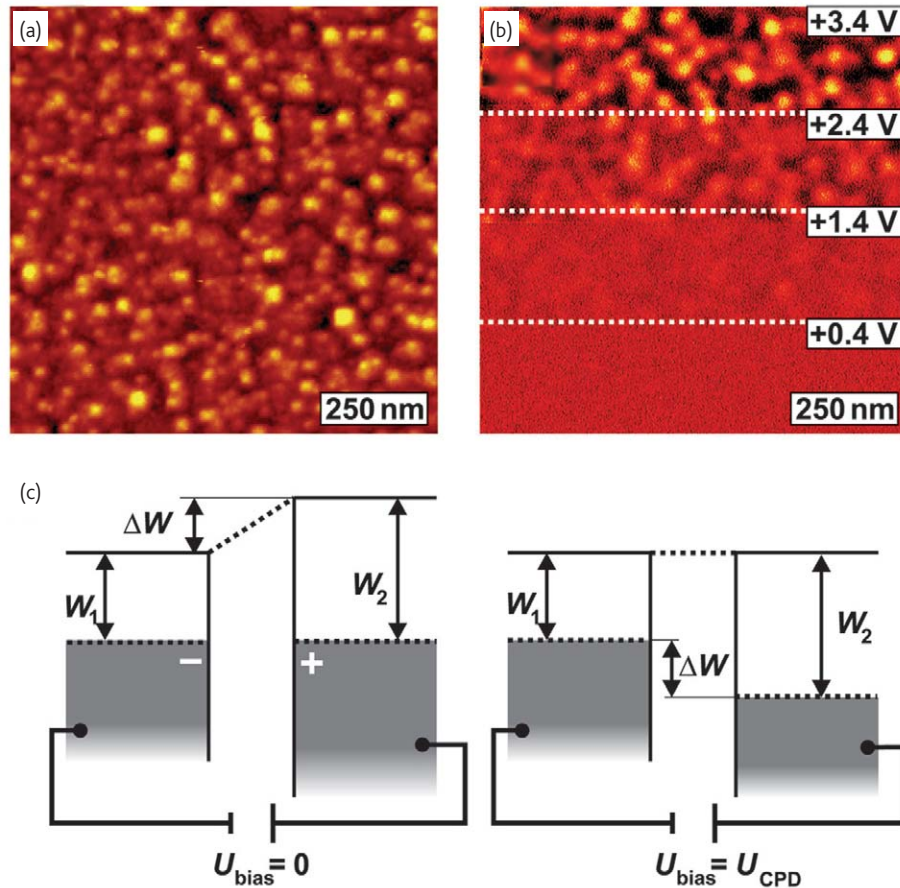
Fig. 2 (a) Surface topography in the constant frequency shift mode ($\Delta f = -0.8$ Hz) with compensated contact potential difference ($U_{Bias} = -U_{CPD} = +0.4$ V). The grainy structure exhibits a root mean square roughness of ~1 nm. The sample ($La_{0.7}Ca_{0.3}MnO_3/LaAlO_3$) is ferromagnetic, but imaged with a nonmagnetic tip. (b) The same area recorded in the plane subtraction mode (h = 10 nm) using the same nonmagnetic tip and four different bias voltages in sections. Only at +0.4 V, i.e. the CPD, are no topography-like features visible. (c) Sketch of the relation between work function $W_1$ and $W_2$ of two materials (e.g. tip and sample), applied bias voltage, and CPD. Compensation is achieved for $eU_{Bias} = \Delta W$.

Electrostatic interactions can also impede MFM image interpretation, if the surface is composed of more than one material of which at least one is ferromagnetic. Let us assume a surface with two components of work functions, $W_1 \neq W_2$. In this situation, it is impossible to compensate the position dependent electrostatic force with a single fixed bias voltage. Further studies are necessary to clarify the true origin of any observed contrast unambiguously. One possibility is to vary $U_{Bias}$ above both components or even employ Kelvin probe microscopy[38]. In the latter case, a lock-in technique is used to compensate for local CPD variations during scanning by adjusting $U_{Bias}$. Another alternative means of distinguishing between magnetostatic and electrostatic contributions is to apply an external magnetic field, which does not influence the electrostatic contrast.

An important consequence of the relatively large tip-sample distance during MFM imaging is a rather weak magnetostatic tip-sample interaction. Therefore, cantilevers with spring constants $c_z$ of ~1–5 Nm$^{-1}$ are used. Softer cantilevers with $c_z < 1$ Nm$^{-1}$ are not advantageous because they exhibit jump-to-contact phenomenon already at relatively large tip-sample distances. In the dynamic mode this instability phenomenon occurs if the attractive force $F_{TS}^{max}$ at the lower turnaround point of the oscillation cycle is larger than $c_zA$. This condition places a lower limit for the scan height during MFM imaging. Furthermore, such cantilevers cannot be used to image the surface topography, which has to be done at even smaller distances and hence larger $F_{TS}^{max}$. The latter is particularly discouraging because it removes one of the merits of MFM, i.e. the ability to obtain the magnetic domain structure and surface topography with high resolution.

## MFM contrast formation

The most important factor for the magnitude of the MFM signal, as well as for the image quality and ease of data interpretation, is the magnetic state of the tip. To address this issue, it is useful to examine the magnetostatic interaction between two macroscopic bodies like the tip and the sample. The interaction energy $E_{TS}$ can be written[39]

$$E_{TS} = -\int \vec{J}_T \vec{H}_S dV = -\int \vec{J}_S \vec{H}_T dV \qquad (1)$$

Both integrals, in which S and T denote sample and tip properties, respectively, are equivalent[40]. Either the sample magnetic stray field $\vec{H}_S$ above the surface is probed with the tip magnetic polarization $\vec{J}_T$ or the sample magnetic polarization $\vec{J}_S$ is probed with the magnetic stray field $\vec{H}_T$ emanating from the tip. Since different distributions of the magnetic polarization in the sample can result in the same stray field above the sample, it is generally impossible to deduce unambiguously the magnetic polarization distribution in the sample from an MFM image without additional knowledge.

If the FM technique (or any other dynamic mode) is used and if the oscillation amplitude $A$ is much smaller than the characteristic decay length of the magnetostatic (or any other) interaction, the force gradient perpendicular to the surface $\partial F_z = \partial z$, i.e. the second derivative of the tip-sample interaction energy, is detected and is related to the measured frequency shift by

$$\partial F_z / \partial z = 2c_z \cdot \Delta f / f_0 \qquad (2)$$

Typically, the decay length of the magnetostatic interaction is ~100 nm. Hence, for oscillation amplitudes on the order of 10 nm or below, eq 2 is valid. To simplify the analysis, we assume that the magnetic structure of the tip can be represented by a dipole $\vec{m}_T = (m_x, m_y, m_z)$ leading to

$$\frac{\partial}{\partial z} F_z = \mu_0 (m_x \frac{\partial^2 H_x}{\partial z^2} + m_y \frac{\partial^2 H_y}{\partial z^2} + m_z \frac{\partial^2 H_z}{\partial z^2}). \qquad (3)$$

It is obvious from eq 3 that image interpretation is easiest if the dipole points only into one direction, e.g. in the z-direction. Then $m_x = m_y = 0$ and the force gradient depends only on the second derivative of the z-component of the sample stray field.

To understand the physical meaning of an MFM image, it is often helpful to use a different representation of eq 1, which is obtained after partial integration[39], i.e.

$$E_{TS} = -\int \rho_S \Phi_T dV - \int \sigma_S \Phi_T dS \qquad (4)$$

Here, $\rho_S = -\text{div}\vec{J}_S$ and $\sigma_S = \vec{n}\vec{J}_S$ are the volume and surface magnetic pole densities, respectively ($\vec{n}$ is the surface normal unit vector). $\Phi_T$ is the scalar potential of the tip stray field $\vec{H}_T$. To obtain the force gradient, $\Phi_T$ has to be replaced by $\partial^2 \Phi_T = \partial z^2$. Eq 4 shows that MFM images reflect the distribution of north and south poles (*magnetic charges*) smoothed by the spatial extent of $\Phi_T$, which is related to the stray field of the tip via $\vec{H}_T = -\vec{\nabla}\Phi_T$.

### Preparing suitable MFM tips

According to the equations evaluated in the section above, the domain structure of MFM tips should be simple (preferably single domain) and their emanating stray fields should be as localized as possible. In
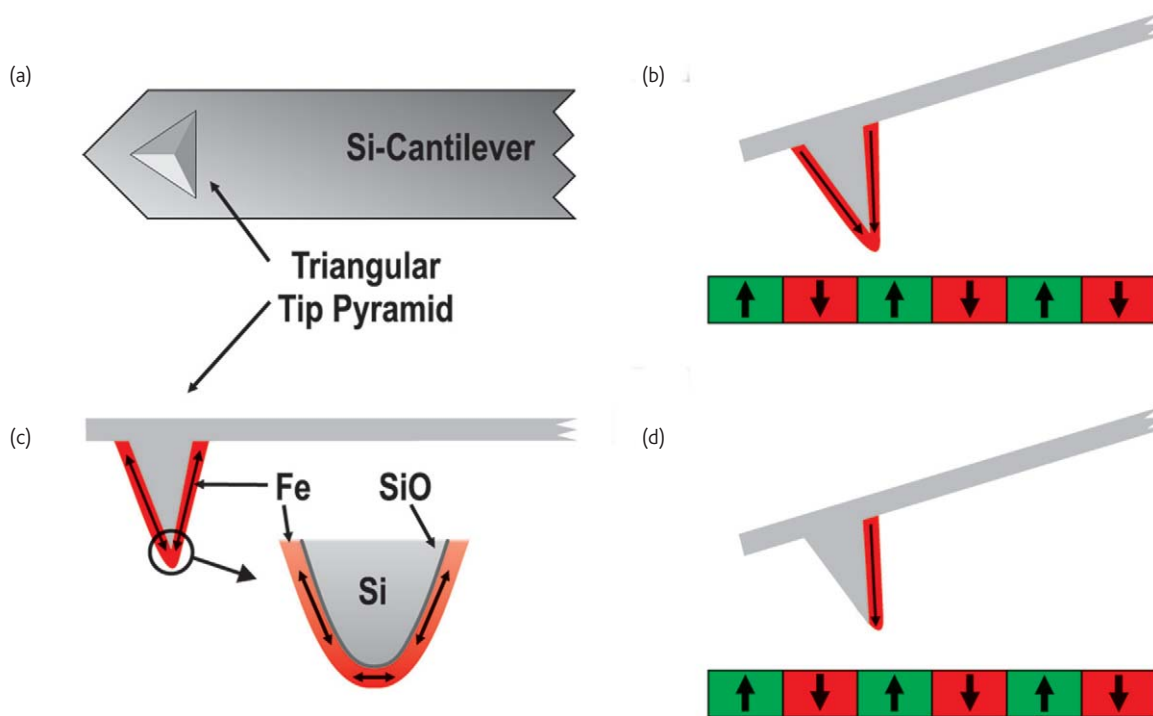


*Fig. 3 (a) A commercial Si cantilever with triangular pyramidal tip. Tip height is ~10 µm. (b) Section along cantilever and Fe-coated tip. The magnification shows the easy axis of magnetization. As a result of shape anisotropy, the easy axis lies everywhere in the plane of the thin Fe film, thus following the tip's profile. (c) Geometric configuration between cantilever, tip pyramid, and sample surface. If the entire tip is coated, the tip exhibits in- and out-of-plane sensitivity ($m_x, m_y, m_z \neq 0$). (d) By only coating the side face perpendicular to the surface, pure out-of-plane sensitivity can be obtained ($m_x = m_y = 0, m_z \neq 0$).*

addition, the magnitude of the stray field must not alter the genuine magnetic structure of the sample, but has to be large enough to produce a detectable signal.

Fig. 3a shows a typical cantilever with a triangular tip. The magnetic structure of a homogeneously Fe-coated tip is dominated by shape anisotropy. Hence, the easy axis of magnetization always lies in the plane of the film following the tip shape, as indicated by the arrows in Fig. 3b. The easy axis is parallel to the surface at the tip apex and, depending on the opening angle and tip-sample geometry, off by 0–30° from the surface normal on the side faces. Because of the change of orientation of the easy axis at the tip apex, a complex domain structure there is likely. Even if such a tip could be treated in an effective dipole approximation, it would exhibit nonzero in-plane, as well as out-of-plane, components ($m_x$, $m_y$, $m_z \neq 0$). Geometrical configuration and magnetization directions of a homogeneously coated tip are displayed in Fig. 3c. For practical purposes, the cantilever is tilted by $\approx 15°$ with respect to the surface. Thus, one side face of the triangular tip pyramid is almost exactly perpendicular to the surface. As shown in Fig. 3d, this situation offers a very convenient and effective way of obtaining a much simpler magnetic structure of the tip by coating only that side face of the pyramid[20]. Thereby, complex domain structures at the tip apex can be avoided and image interpretation becomes easier, because only $m_z$ is nonzero. In addition, the stray field of such tips is more localized, leading to a higher spatial resolution. Magnetic properties of the tips can also be modified by varying the material, e.g. by depositing Co, Ni, or ferromagnetic alloys. However, all data shown in this review are obtained with Fe-coated tips.

Fig. 4a,b compares the contrast obtained with two different tips on a sample with isolated circular out-of-plane polarized magnetic domains. These domains were generated by applying a magnetic flux density of 0.295 T close to the saturation magnetic polarization of a sample comprising a $La_{0.7}Sr_{0.3}MnO_3$ (LSMO) layer on a $LaAlO_3$ (LAO) substrate and are polarized antiparallel to $B$ and antiparallel to the z-component of the magnetic polarization of the tip. Hence, these domains appear dark. Although $B$ is equal in Fig. 4a and 4b, the density of the dark regions is not the same because the magnetic history is different. The tip in Fig. 4a exhibits a mixed out-of-plane and in-plane sensitivity, i.e. $m_x$, $m_y$, and $m_z$ are all nonzero. Such tips generate an additional characteristic crescent-shaped contrast that is absent, if, as in Fig. 4b, a pure out-of-plane sensitive tip (only $m_z \neq 0$) is used. Clearly, Fig. 4b is much easier to interpret than Fig. 4a and can be directly related to the magnetic structure of the sample shown below the images in Fig. 4. Note that the bulk saturation magnetic polarization $J_{Sat}$ of Fe is 2.187 T, hence the tip is not fully aligned in the applied flux density of 0.295 T because of the strong shape anisotropy.
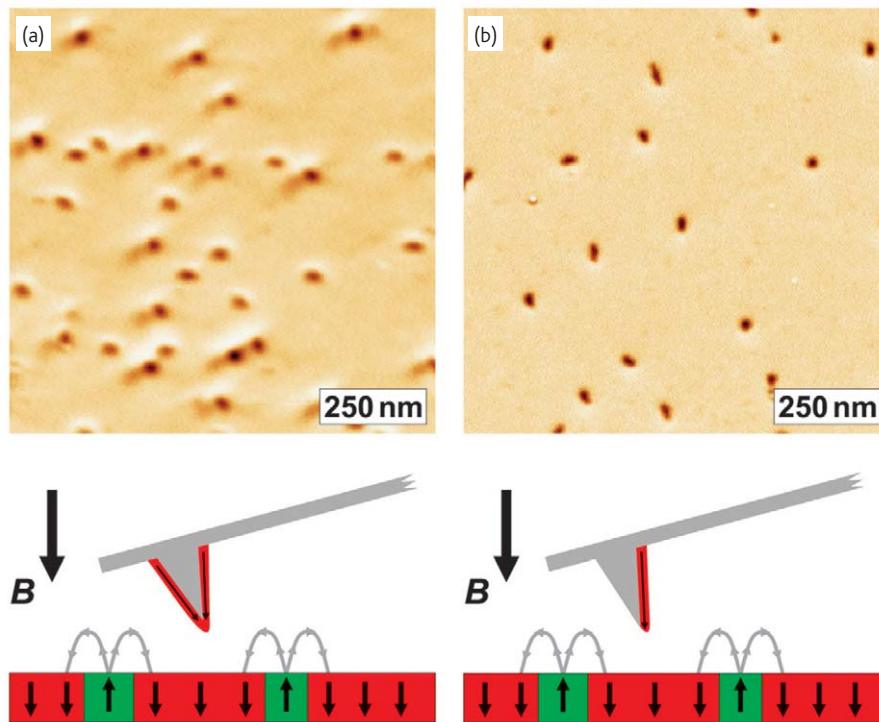


Fig. 4 (a) MFM tip with mixed out-of- and in-plane sensitivity. (b) MFM tip with pure out-of-plane sensitivity. Both images were recorded at 5.1 K in the constant height plane subtraction mode in B = 0.295 T. Since the magnetic history is not identical, the density of dark domains is different in (a) and (b). The magnetic configuration of tip and sample ($La_{0.7}Ca_{0.3}MnO_3/LaAlO_3$) relative to B is shown below the images. Image (b) reflects the circular domains much better than (a), which exhibits a destinctive crescent-shaped contrast.
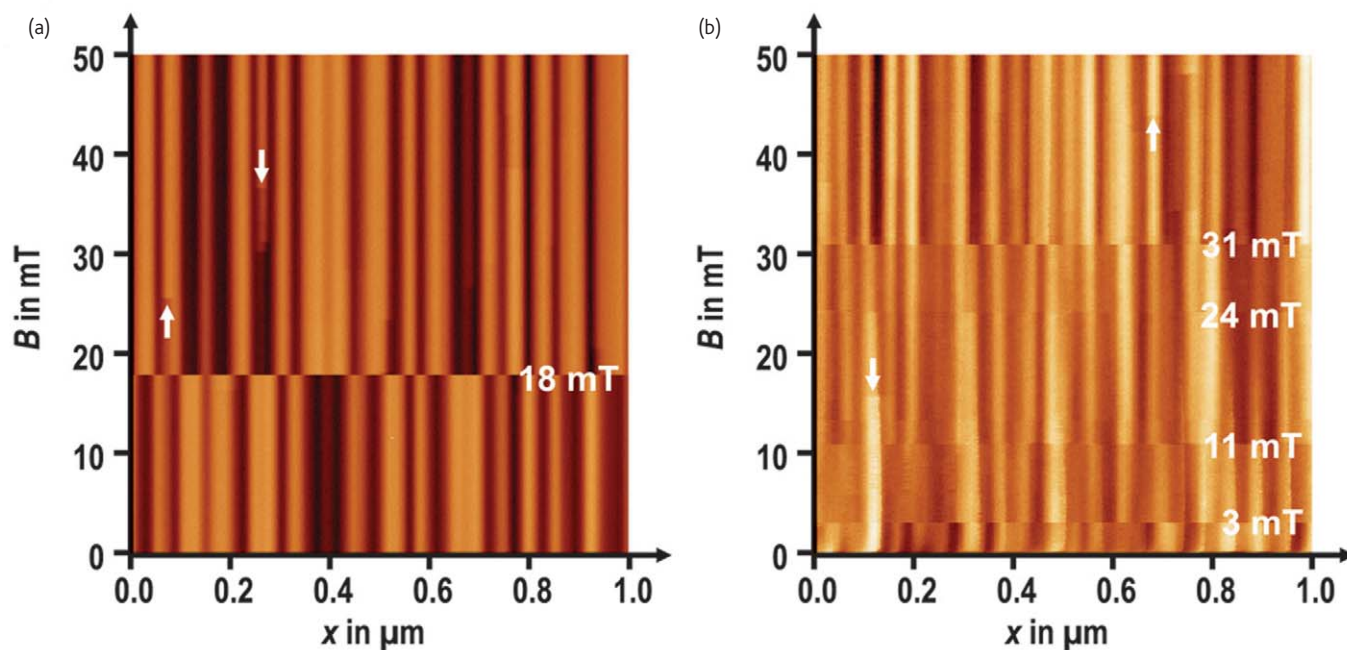
Fig. 5 (a) Well-behaved single domain tip. (b) Tip with a complex domain structure at the tip apex. In both cases the tip is scanned in the constant height plane subtraction mode along one scan line at 5.1 K, while B is ramped from 0 mT to 50 mT on a sample (La$_{0.7}$Ca$_{0.3}$MnO$_3$/LaAlO$_3$) with out-of-plane anisotropy. The contrast in (a) inverts from one line to the next only at 18 mT. On the other hand, four contrast jumps at 3 mT, 11 mT, 24 mT, and 31 mT are visible in (b). Changes within a single vertical stripe (see arrows) are magnetization jumps of the sample and not related to the tip.

In addition, we have found that tips prepared as shown in Fig. 3d behave like single-domain tips, indicating that at least the relevant front part of the tip apex is composed of only one domain. This is demonstrated in Fig. 5. The tip is scanned along the same line on a sample with out-of-plane anisotropy, while the external flux density is steadily increased from 0–50 mT. Thus, the oppositely polarized domains are represented by vertical stripes. Contrast changes within an individual stripe (see arrows) mark magnetic polarization reversals of the sample. On the other hand, at ~18 mT, where the contrast abruptly inverts in all stripes simultaneously on a single line, the magnetic polarization of the tip is switched by 180°. Tips prepared as shown in Fig. 3c do behave differently. They change their contrast in an irregular fashion upon field variations and often several discrete contrast changes are observed before the tip is completely switched.

Another important issue is tip-induced perturbations of the sample's genuine magnetic structure, which should be avoided to facilitate easy image interpretation (in principle, the opposite is also possible and should be prevented as well). The magnitude of the magnetostatic tip-sample interaction depends on the strength of the tip's stray field on the sample surface, which can be adjusted by the tip-sample distance, the material deposited onto the tip, and the film thickness. Setting large tip-sample separations is a bad choice because then the tip's stray field at the surface is less localized, thereby decreasing the spatial resolution. The best approach is to optimize the film thickness for a given tip material and specimen. The optimal thickness leads to the largest possible MFM signal without modifying the genuine domain pattern of the sample. The latter can be identified by glitches along scan lines.

## Resolution of MFM

To demonstrate the resolution capabilities of MFM, we present data obtained on a ferromagnetic thin film with out-of-plane anisotropy. The sample is an 80-nm-thick LSMO film prepared on a (001) LAO substrate by pulsed laser deposition. LSMO/LAO film growth is epitaxial, but because of a lattice mismatch of 2.4% ($a_{LAO}$ < $a_{LSMO}$), the film is compressively stressed in the ab plane and exhibits an extended c lattice parameter[41]. In order to relax this stress, misfit dislocations are formed in a rectangular pattern along main crystallographic axes[42]. Above a thickness of ~70 nm, the film breaks up into rectangular columns of 20–35 nm in size, separated by amorphous grain boundaries[43]. The distortion of the unit cell leads to an easy axis of magnetization perpendicular to the film plane. The resulting maze-type domain pattern is visible in Fig. 6.

The characteristic domain width in Fig. 6a is ~80 nm. However, the actual resolution of MFM is one order of magnitude better, as demonstrated in the following experiment. Fig. 7a,b displays two images recorded at an external flux density B of 275 mT and 270 mT, respectively. Bright areas, which are parallel to B, cover most of the images. Subtracting one image from the other reveals those regions that have reversed their magnetization direction upon changing the
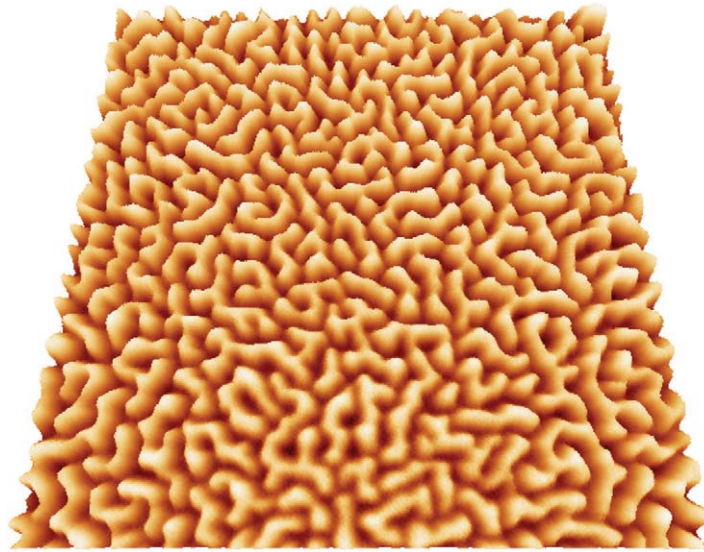
Fig. 6 (a) Remanent domain structure of $La_{0.7}Sr_{0.3}MnO_3$ grown epitaxially on $LaAlO_3$ (001). The 4 µm × 4 µm image was recorded at 5.1 K in the constant height plane subtraction mode (h = 24 nm) using a tip coated with 5 nm Fe on one side face as shown in Fig. 3d. The typical maze-type pattern is clearly visible. Bright and dark areas indicate parallel and antiparallel alignment between tip and sample magnetizations, respectively.

magnitude of B. Hence, all features in the final image, Fig. 7c, are of unambiguously magnetic origin. The size of the observed discrete magnetization jumps varies over several orders of magnitude[19]. Radii of the smallest detected reversed regions in Fig. 7c are ~15 nm (see arrows), proving the nanoscale spatial resolution of MFM. On the same sample, even regions with radii below 10 nm can be identified[19]. However, improving the resolution further, e.g. to the atomic scale, is not feasible using standard MFM data acquisition schemes. As with all scanning probe near-field methods, the achievable resolution depends on the effective probe size and the tip-sample separation. For MFM, the latter is simply the adjusted scan height h, while the effective probe size is given by the localization of the emanating stray field of the tip.

## MExFM: imaging spin configurations
### Prerequisites for magnetic sensitivity with atomic resolution

Following the argument above, atomic resolution can only be achieved if a tip is atomically sharp and the tip-sample distance is on the order of interatomic distances, i.e. below 0.5 nm. This situation is routinely realized during atomic resolution imaging in the constant frequency shift mode using the FM technique in the NC regime (FM-AFM or NC-AFM)[35]. At such small tip-sample distances, cantilevers with relatively large spring constants ($c_z > 10$ Nm$^{-1}$) are required to avoid jump-to-contact phenomenon. The arrangement of atoms on a surface can then be detected via the electron-mediated chemical interaction between the tip and the sample[36]. To detect
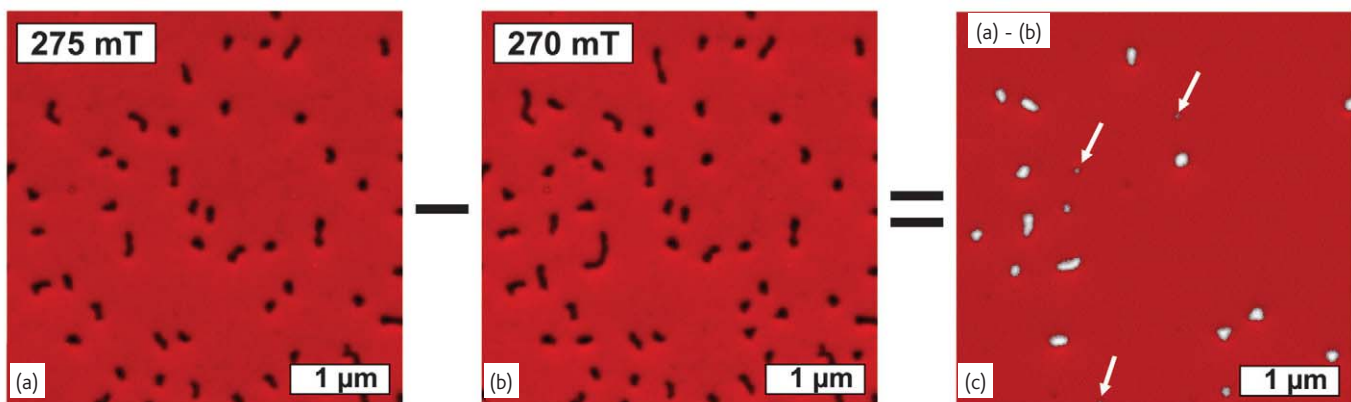


Fig. 7 (a), (b) The domain pattern at 5.1 K in two slightly different external magnetic flux densities, B, of 275 mT and 270 mT, respectively. At these flux densities most of the sample is magnetized parallel to B and thus appears bright. The subtracted image (c) = (a) − (b) reveals the regions in which the magnetization is reversed by 180°. The radii of the smallest reversed regions are ~15 nm and marked by arrows.

the arrangement of magnetic moments on a surface with atomic resolution, i.e. performing MExFM, the same setup can be used. However, it is also required that the foremost tip atom carries a stable magnetic moment, which interacts via the short-range spin-dependent magnetic exchange interaction with the sample's magnetic moments. We have recently demonstrated the feasibility of MExFM under these conditions[10].

To detect a magnetic contrast on the atomic scale unambiguously, the magnetic exchange interaction has to be separated from the chemical interaction. This corresponds to a separation between surface topography and domain structure in MFM. However, simply scanning at a larger tip-sample separation is not a solution because chemical and magnetic exchange interactions are electron mediated with similar decay lengths on the order of ~0.1 nm. While it is possible to compensate the electrostatic forces in MFM experiments, this is not an option on the atomic scale. For ferromagnetic samples, field-dependent experiments could be performed to separate magnetic

exchange and chemical interactions. However, one has to keep in mind that an external magnetic field can change the spin configurations of both the tip and sample. Nevertheless, domain walls, or any other magnetic structure where the spin direction varies on the atomic scale, can be investigated in a straightforward way. For example, in antiferromagnetic samples where chemically identical atoms carry spins that point into opposite directions, this complication is completely absent. Moreover, antiferromagnets do not possess a magnetic stray field and their spin configuration is much less affected by an external magnetic field than that of ferromagnets.

## MExFM on the antiferromagnetic insulator NiO(001)

A prototypical sample system in this respect is the antiferromagnetic insulator NiO(001). Its structural and magnetic properties are well known. Moreover, theoretical calculations regarding MExFM experiments on this system already exist[27]. Chemical and spin structure of NiO are shown in Fig. 8a. It crystallizes in the rocksalt
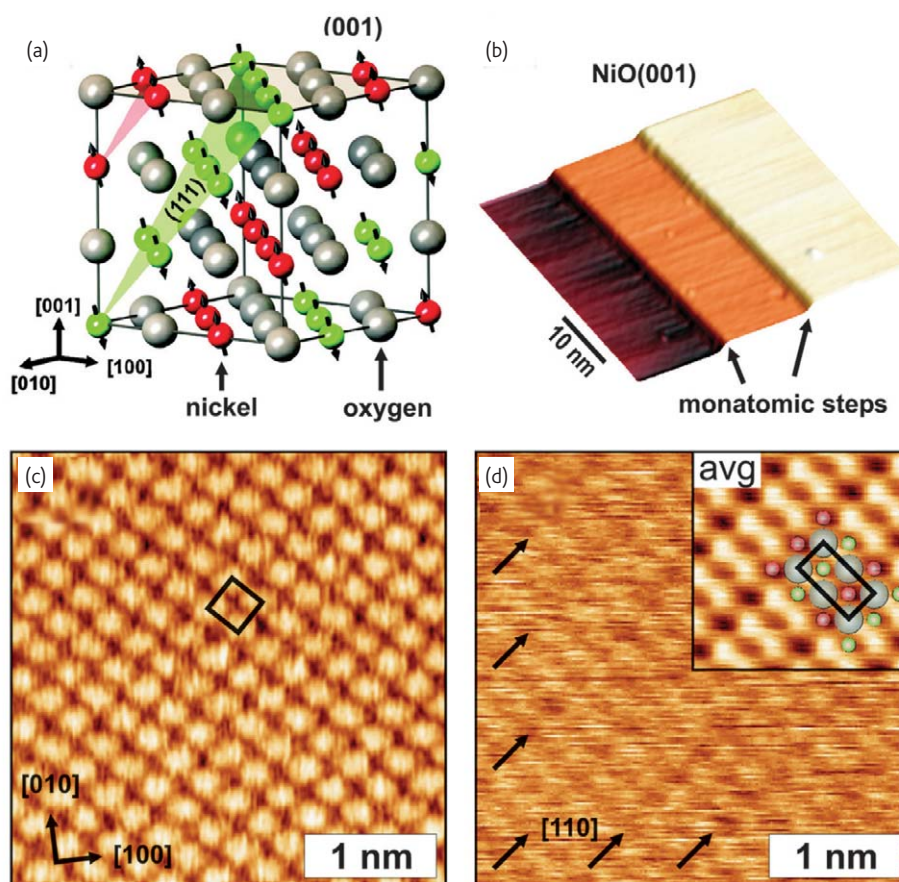


Fig. 8 (a) Chemical and magnetic structure of NiO. (b) Topography of NiO(001) after cleavage. Image acquisition was performed in the constant frequency shift mode ($\Delta f = -1.3$ Hz) and shows atomically flat terraces separated by monatomic steps. (c) Atomic resolution with chemical contrast on NiO(001). The AFM image was recorded with a nonmagnetic tip at 8.1 K and $\Delta f = -11$ Hz. Protrusions and depressions correspond to O and Ni atoms, respectively. The square indicates the $(1 \times 1)$ surface unit cell. (d) MExFM image of NiO(001) using an Fe-coated tip at 7.9 K and $\Delta f = -23.4$ Hz in an external flux density of $B = 5$ T. As in (b), chemical resolution is obtained. In addition, a contrast modulation on neighboring rows of depressions (Ni atoms) clearly proves the simultaneous detection of the magnetic exchange interaction between tip and sample spins. The inset in (c) is obtained after unit cell averaging of the raw data.

structure with $a$ = 417 pm. The (001) cleavage plane remains unreconstructed and exhibits only a slight rumpling[44]. Clean and well-defined (001) surfaces can be obtained by *in situ* cleavage, as shown in Fig. 8b. The topography is dominated by atomically flat terraces separated by monatomic steps. While for MFM even relatively rough surfaces are suitable, imaging with atomic resolution requires well defined surfaces.

Fig. 8c shows that the configuration of Ni and O atoms in the (1 × 1) surface unit cell can be resolved if imaging is performed with an atomically sharp tip. The square indicates the size of the (1 × 1) surface unit cell. In constant frequency shift images with atomic resolution, as in Fig. 8c, protrusions and depressions indicate stronger and weaker short-range interactions, respectively. Since the chemical interaction is electron mediated[45], protrusions represent positions of increased valence charge density. Hence, protrusions and depressions can be identified as O and Ni atoms, respectively, because NiO is an ionic crystal in which charge is transferred from Ni to O.

The magnetic properties of NiO are determined by the strongly localized d-electrons of the Ni atoms. They couple antiferromagnetically via superexchange across bridging O atoms. Within a given {111} plane, spins order ferromagnetically but neighboring {111} planes order antiferromagnetically. Hence, the (001) surface exposes a row-wise antiferromagnetic structure exhibiting a (2 × 1) magnetic surface unit cell with canted magnetic moments pointing in <211> directions. This configuration is clearly reflected by the atomic scale contrast visible in Fig. 8d, recorded using a tip homogeneously coated with Fe. The rectangle indicates the (2 × 1) magnetic surface unit cell. As in Fig. 8c, protrusions represent O atoms and depressions Ni atoms. However, neighboring rows of Ni atoms exhibit a different contrast. Since they are chemically and structurally identical, the observed difference must be of magnetic origin. The magnetostatic dipole interaction between two atomic magnetic moments at distances on the order of 0.5 nm or below is much weaker (~10 eV) compared with the magnetic exchange interactions between them (~10 meV). Thus, it can be inferred that the obtained atomic-scale contrast does indeed stem from the short-range magnetic exchange force between the tip and sample spins.

We have found that a smaller tip-sample distance than for pure chemical contrast is needed to obtain an MExFM signal[10]. This indicates that a direct exchange between the spin-carrying d-electrons of the Fe tip and the localized d-electrons of the Ni atoms seems to be necessary. The chemical contrast occurs at larger separations via the s- and p-electrons, which reach farther into the vacuum region. If the magnetic exchange were indirect, e.g. via polarization of s- and p-electrons, one would expect that the chemical and magnetic exchange contrast would appear at the same tip-sample distance via polarization of the s- and p-electrons. In addition, we conclude that superexchange does not play a role because no contrast between neighboring O rows is observed in Fig. 8d.

## Controlling the spin direction at the tip apex

As for MFM, controlling the magnetic properties of the tip is crucial. For MExFM the relevant part of the tip is the foremost atom at the tip apex. Therefore, it is necessary to coat the tip apex with Fe and not only one side face. Note that a complex domain structure is not a problem in MExFM experiments because only the spin of the foremost tip atom really matters.

One way to describe the magnetic exchange interaction between spins is the Heisenberg model:

$$H_{ij} = -\sum_{ij} J_{ij}\, \vec{S}_i \vec{S}_j \tag{5}$$

where $H$ is the Hamiltonian, i.e. the interaction energy, and $J_{ij}$ is the exchange integral, which determines strength and type (ferro- or antiferromagnetic) of the coupling between the spins $\vec{S}_i$ and $\vec{S}_j$. Its physical origin is the Coulomb interaction between electrons and the Pauli Exclusion Principle of indistinguishable particles.

It should be mentioned that height variations on the atomic scale in constant frequency shift images cannot be directly related to the force gradient because, unlike MFM, the amplitude is not much smaller but much larger than the decay length of the relevant interaction. Obtaining the magnitude of the tip-sample interaction energy (or force or force gradient) requires distance dependent measurements, i.e. force spectroscopy. This has been done on NiO(001) to determine the magnitude of the chemical interaction force[30,31], which is on the order of 1 nN, but not yet with spin sensitivity. Theory predicts magnetic exchange forces on the order of a few 0.1 nN between NiO(001) and an Fe tip[27]. However, caution has to be exercised regarding this value because the tip consists of only a single Fe atom and no relaxation effects are included. For chemical interactions, it has been found that significant relaxations take place in the tip and sample[36] and have to be included to calculate the correct magnitude of the tip-sample interaction.

Considering, for simplicity, only the spin $\vec{S}_T$ of the foremost tip atom and the spin $\vec{S}_S$ of the sample atom directly underneath, eq 5 allows us to infer that the magnitude of the MExFM signal depends on the angle between $\vec{S}_T$ and $\vec{S}_S$. The largest signal is expected if they are either parallel or antiparallel. Since the magnetic moments of Ni are canted with respect to the (001) plane, such a situation is difficult to realize. As indicated in Fig. 3b, the easy axis of magnetization of the tip is parallel to the surface at the apex. Thus, the spin of the foremost tip atom is also likely to be in-plane, as shown in Fig. 9a. Even though the azimuthal, as well as the polar angle, of the canted spins of the Ni atoms depend on the type of antiferromagnetic domain on which imaging is performed, they always possess an in-plane component. Nevertheless, many unfavorable relative orientations between tip and sample spins do exist because the direction of the tip's magnetic polarization within the plane parallel to the surface is arbitrary. In the worst case, the in-plane components of the interacting tip and sample spins are perpendicular to each other, whereby the

magnetic signal vanishes. In this respect, it is much better to prepare tips with spins perpendicular to the surface, because then the out-of-plane components of tip and sample spins can only be either parallel or antiparallel, meaning that we always will find a nonvanishing interaction. One way to achieve this is to apply a magnetic flux density $B$ perpendicular to the surface that is larger than the saturation magnetic polarization of the ferromagnetic tip material ($J_{Sat} = 2.187$ T for Fe). For that reason, the image in Fig. 8b has been recorded in an external flux density of 5 T, resulting in a situation as shown in Fig. 9b. Note that the antiferromagnetic structure of the sample remains unaltered even if exposed to a flux density of 5 T.

Aligning the spins at the tip apex into a favorable direction seems to be very important considering the numerous unsuccessful reports of MExFM experiments on NiO(001) with ferromagnetic tips but in zero field[28–31]. It should be mentioned that some of our experiments indicate that the spin at the foremost tip atom is not fully aligned by an external flux density, even if $B > J_{Sat}$[46]. In this context, it is important to remember that $J_{Sat}$ is a bulk property, while the exposed foremost tip atom is certainly not in a bulk-like environment. Local anisotropies can be large enough to result in a noncollinear alignment between the spin of the foremost tip atom and the direction of $B$. However, an external flux density will facilitate spin alignment in its direction, thereby the MExFM signal can be maximized. Note that this finding is irrelevant for MFM because the stray field of an MFM tip stems from a large number of ferromagnetically coupled spins in the film, which all point into the same direction. A few misaligned spins at the tip apex do not have a significant impact on MFM contrast formation.

## Future perspectives

The breakthrough experiment on NiO(001) opens new possibilities for magnetic imaging on the atomic scale. Until now, a similar resolution could only be achieved with spin-polarized scanning tunneling microscopy (SP-STM)[47], but like all STM-based methods was limited to conducting samples. Hence, spin configurations of insulators, although a very important class of materials, could not be investigated until very recently. For example, NiO and similar antiferromagnetic insulators are often used in exchange bias systems[48]. Studying them on the atomic level could provide insight into the unsolved problem of the magnitude of the exchange bias effect, which might be related to uncompensated spins at the interface.

Insulators, magnetic or nonmagnetic, also serve as important substrates for magnetic molecules or adatoms. On metals, adsorbed molecules or adatoms couple strongly to the substrate, which significantly alters their electronic as well as magnetic properties. If STM (or SP-STM) has to be used, only ultrathin insulating layers can be used for partial decoupling[49]. Now, magnetic properties of individual magnetic molecules and atoms can be studied even on bulk insulators, where the decoupling is complete because of the large bandgap.

Using a force microscopy setup, it is also possible to measure dissipative processes by monitoring the excitation amplitude necessary to keep the cantilever oscillation amplitude $A$ constant. Atomic-scale dissipative processes have been related to phonon excitation[50] or adhesion hysteresis[51,52]. On magnetic samples, spin excitation (magnons) offer an additional dissipative channel that might be accessible by MExFM. Another important data acquisition scheme is force spectroscopy, which provides quantitative information about
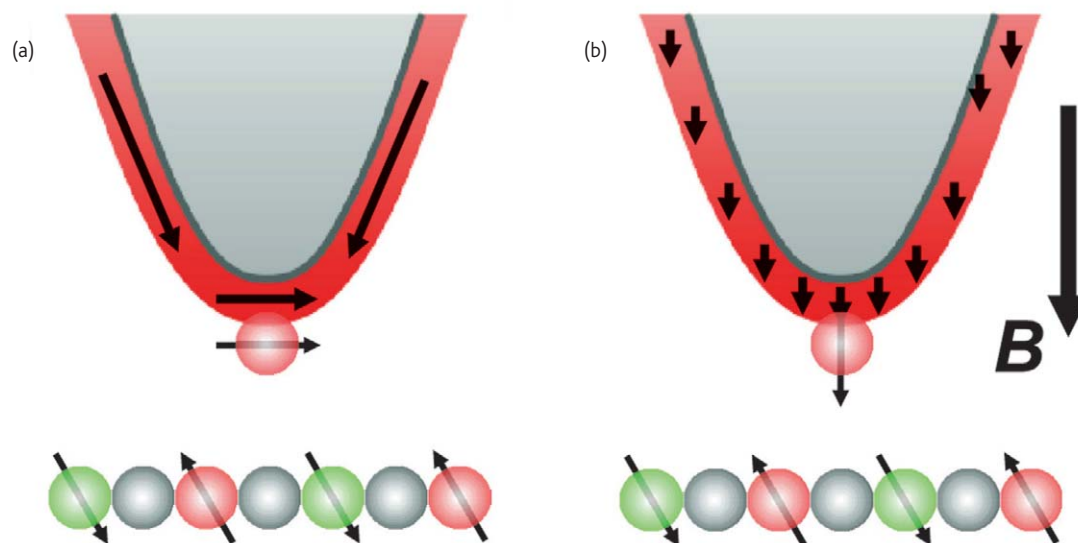


Fig. 9 (a) Most likely configuration of the spin of the foremost tip atom at B = 0 T. Its orientation coincides with the easy axis of magnetization at the tip apex according to Fig. 3b. (b) Most likely configuration of the spin of the foremost tip atom if B > J_Sat. The magnetic polarization is fully aligned parallel to B. The latter configuration is much more suitable if samples like NiO(001) with canted surface spins are studied. However, both cases do not necessarily reflect the actual situation at the tip apex. Even if B > J_Sat, local anisotropies could result in a spin direction that is not collinear with B.

the magnitude and distance dependence of the tip-sample force on specific atomic sites[30,53]. Thereby, the magnitude of the magnetic exchange interaction can be determined. If the interaction is not direct but RKKY-like (Ruderman–Kittel–Kasuya–Yosida), even the expected oscillatory behavior might be observable. Comparing the present situation with the rapid developments in SP-STM experiments[9,54–56], we can expect a similar wealth of interesting MExFM experiments in the years to come.

With MExFM, the ultimate limits of force-based magnetic resolution is reached. However, it will not replace MFM because atomic resolution usually requires well-defined, atomically flat surfaces, which are rarely present on real devices. In general, more than one tip atom is close to rough surfaces, and those atoms that are closest to the surface change during scanning because the local geometry between the tip apex and the surface changes. It will also be difficult to maintain a small and stable tip-sample separation below 0.5 nm if large areas have to be scanned, which would be necessary for domain imaging

with MExFM. Moreover, MFM can also be performed on ferromagnetic surfaces, which are covered by a nonmagnetic layer. This might be a nonmagnetic oxidation layer, which is often formed in ambient conditions, or a protection layer against oxidation.

In summary, the combination of nanoscale magnetic resolution, minimum sample preparation, and simultaneously available high-resolution topographic data offered by MFM is still unique. Hence, MFM will remain a very useful tool for the study of the magnetic properties of nanotechnologal devices. On the other hand, MExFM can be expected to provide valuable information about magnetic interactions on the molecular and atomic level.  `nt`

## Acknowledgments

### REFERENCES

1. Bitter, F., *Phys. Rev.* (1932) **41**, 507
2. Hubert, A., and Schäfer, R., *Magnetic domains: the analysis of magnetic microstructures*, Springer, (2000), 24
3. Chapman, J. N., *J. Phys. D: Appl. Phys.* (1984) **17**, 623
4. Oepen, H. P., and Kirschner, J., *Scanning Microsc.* (1991) **5**, 1
5. Schneider, C. M., *J. Magn. Magn. Mater.* (1996) **156**, 94
6. Chang, A. M., *et al.*, *Appl. Phys. Lett.* (1992) **61**, 1974
7. Kirtley, J. R., and Wikswo, J. P., Jr., *Annu. Rev. Mater. Res.* (1999) **29**, 117
8. Hartmann, U., *Annu. Rev. Mater. Res.* (1999) **29**, 53
9. Bode, M., *Rep. Prog. Phys.* (2003) **66**, 523
10. Kaiser, U., *et al.*, *Nature* (2007) **446**, 522
11. Binnig, G., *et al.*, *Phys. Rev. Lett.* (1986) **56**, 930
12. Wadas, A., *et al.*, *Appl. Phys. Lett.* (1994) **64**, 1156
13. Löhndorf, M., *et al.*, *Appl. Phys. Lett.* (1996) **68**, 3635
14. Schneider, M., *et al.*, *J. Appl. Phys.* (1996) **79**, 8578
15. Shinjo, T., *et al.*, *Science* (2000) **289**, 930
16. Moser, A., *et al.*, *Phys. Rev. Lett.* (1995) **74**, 1847
17. Volodin, A., *et al.*, *Appl. Phys. Lett.* (1998) **73**, 1134
18. Liebmann, M., *et al.*, *Rev. Sci. Instrum.* (2002) **73**, 3508
19. Schwarz, A., *et al.*, *Phys. Rev. Lett.* (2004) **92**, 077206
20. Liebmann, M., *et al.*, *Phys. Rev. B* (2005) **71**, 104431
21. Schwarz, A., *et al.*, *Appl. Phys. Lett.* (2006) **88**, 012507
22. Pi, U. H., *et al.*, *Phys. Rev. B* (2006) **73**, 144505
23. Wiesendanger, R., *et al.*, *J. Vac. Sci. Technol. B* (1991) **9**, 519
24. Mukasa, K., *et al.*, *Jpn. J. Appl. Phys.* (1994) **33**, 2692
25. Nakamura, L., *et al.*, *Jpn. J. Appl. Phys.* (1998) **37**, 6575
26. Foster, A. S., and Shluger, A. L., *Surf. Sci.* (2001) **490**, 211
27. Momida, H., and Oguchi, T., *Surf. Sci.* (2005) **590**, 42
28. Hoffmann, R., *et al.*, *Phys. Rev. B* (2003) **67**, 085402
29. Hosoi, H., *et al. Nanotechnology* (2004) **15**, 505
30. Hölscher, H., *et al.*, *Appl. Phys. Lett.* (2002) **81**, 4428
31. Langkat, S. M., *et al.*, *Surf. Sci.* (2003) **527**, 12
32. Si cantilevers SSS-NCL and PPP-NCL from Nanosensors, www.nanosensors.com
33. Albrecht, T., *et al.*, *J. Appl. Phys.* (1991) **69**, 668
34. Giessibl, F.-J., *Science* (1995) **267**, 68
35. Morita, S., *et al.*, (eds.), *Noncontact Atomic Force Microscopy*, Springer, (2002)
36. Pérez, R., *et al.*, *Phys. Rev. Lett.* (1997) **78**, 678
37. Dreyer, M., *et al.*, *Appl. Phys. A* (1998) **66**, S1209
38. Nonnenmacher, M., *et al.*, *Appl. Phys. Lett.* (1991) **58**, 2921
39. Hubert, A., *et al.*, *Phys. Status Solidi B* (1997) **204**, 817
40. Wright, C. D., and, Hill, E. W., *Appl. Phys. Lett.* (1995) **67**, 433
41. Kwon, C., et. al., *J. Magn. Magn. Mater.* (1997) **172**, 229
42. Van Tendeloo, G., *et al.*, *J. Magn. Magn. Mater.* (2000) **211**, 73
43. Jiang, J. C., *et al.*, *Appl. Phys. Lett.* (2002) **80**, 4831
44. Okazawa, T., *et al.*, *Phys. Rev. B* (2003) **67**, 195406
45. Ciraci, S., *et al.*, *Phys. Rev. B* (1990) **41**, 2763
46. Kaiser, U., *et al.*, unpublished data
47. Heinze, S., *et al.*, *Science* (2000) **288**, 1805
48. Nogués, J., and, Schuller, I. K., *J. Magn. Magn. Mater.* (1999) **192**, 203
49. Heinrich, A. J., *et al.*, *Science* (2004) **306**, 466
50. Gauthier, M., and Tsukada, M., *Phys. Rev. B* (1999) **60**, 11716
51. Trevethan, T., and Kantorovich, L., *Nanotechnology* (2004) **15**, S34
52. Hoffmann, R., *et al.*, *Nanotechnology* (2007) **18**, 395503
53. Lantz, M. A., *et al.*, *Science* (2001) **291**, 2580
54. Bode, M., and Wiesendanger, R., Spin-Polarized Scanning Tunneling Microscopy. In *Modern Techniques for Characterizing Magnetic Materials*, Zhu, Y., (ed.), Springer, (2005)
55. Bode, M., and Wiesendanger, R., Spin-Polarized Scanning Tunneling Spectroscopy. In *Magnetic Microscopy of Nanostructures*, Hopster, H., and Oepen, H. P., (eds.), Springer, (2005)
56. Schwarz, A., *et al.*, Scanning Probe Techniques: MFM and SP-STM. In *Handbook of Magnetism and Advanced Magnetic Materials*, Kronmüller, H., and Parkin, S., (eds.), Wiley, (2007), **3**